J Appl Electrochem (2008) 38:1065–1073
DOI 10.1007/s10800-008-9539-x

ORIGINAL PAPER

Computer simulation of the effective double layer occurring on a catalyst surface under electro-chemical promotion conditions

E. P. M. Leiva · C. Vázquez · M. I. Rojas · M. M. Mariscal

Received: 10 December 2007 / Revised: 27 February 2008 / Accepted: 27 February 2008 / Published online: 5 June 2008

Abstract In this work, the structural and energetic properties of two typical catalytic surfaces, Na/Pt(111) and O/Pt(111), are studied by means of quantum mechanical calculations and Monte Carlo Grand Canonical simulations. The simulations were performed with electrostatic potentials at different truncation schemes. In order to elucidate the modification of catalyst surfaces produced by the backspillover of ionic species onto Pt(111), the electrostatic field at the interface due to the electric double layer was also analyzed.

Keywords Electrochemical promotion · NEMCA effect · Computer simulations · Quantum mechanical calculations

1 Introduction

The catalytic activity of some metallic surfaces deposited on solid electrolytes, may be reversibly decreased or accelerated by means of the electrochemical pumping of ions to the catalyst/gas (c/g) interface. This type of modification is named NEMCA effect (Non Faradaic Electrochemical Modification of Catalytic Activity) [1]. Depending on the nature of the solid electrolyte and the potential program applied to the electrochemical interface, different types of ions may be backspilled there. In the case of O^{-2} conductors like Ytria-Stabilized-Zirconia (YSZ), the positive polarization of the electrochemical interface leads to the formation of strongly polarized oxygen species, denoted with $O^{\delta-}$ that migrate to the c/g interface. On the other hand, when Na^{+} conductors are employed like β''-Al_2O_3, the negative polarization of the electrode leads to the migration of strongly polarized metal atoms usually represented as $Na^{\delta+}$. These strongly polarized species play a decisive role in the catalysis of reactions at the c/g interface and have been visualized in scanning tunnelling microscopy experiments [2, 3]. Thus, an effective double layer is established, which modifies the work function of the metal exposed and affects the binding strength of the reacting adsorbed molecules. The change in the surface dipole of the catalyst, manifest in the change of the work function of the system, produces remarkable changes in the surface catalytic activity that are reversible and even predictable on the basis of models [4–6].

According to mathematical modelling developed to explain different aspects of electrochemical promotion [7], the electrostatic field generated by the backspilled species plays a decisive role in the catalysis determining, together with the dipolar properties of the reactants, the electrochemical promotion behaviour. Thus, knowledge of the field distribution at the c/g interface represents an important part of the problem under consideration.

In the present work, we attempt to contribute to the understanding of the NEMCA effect by taking account of different potentially promoting species in terms of Density Functional Theory (DFT) calculations. A scheme using Monte Carlo (MC) simulations in the Grand Canonical ensemble μVT was also devised with the purpose of using it in the future to the analysis of the role of the coverage degree of the promoting species. These simulations are primarily devoted to emulating the adsorption of Na^{+} ions on a charged surface. The structure of the system, the coverage degree and the surface dipole were analyzed as function of the chemical potential.

E. P. M. Leiva (✉) · C. Vázquez · M. I. Rojas · M. M. Mariscal
INFIQC, Unidad de Matemática y Física, Fac. de Ciencias Químicas, Universidad Nacional de Córdoba, Ciudad Universitaria, 5000 Cordoba, Argentina
e-mail: eleiva@fcq.unc.edu.ar

Concerning the DFT calculations, we studied O-$p(2 \times 2)$–Pt(111); Na-$p(2 \times 2)$–Pt(111) Na-$p(4 \times 4)$–Pt(111) and Na-$p(4 \times 4)$/O-$p(2 \times 2)$/Pt(111) ordered structures. The energetic of the system was considered, and the charge distribution at the interface was evaluated through the Mulliken population analysis [8]. The adsorption of some of the O species leads to a considerable strain of the Pt(111) surface. We also investigate the change of the electronic density, electrostatic potential and electric field of the interface upon formation of the charged double layer.

Certain aspects of the comparison of these results with experiment data once need to be highlighted. On the one hand, we consider equilibrated systems, in the sense that the status of adsorbed species is not altered by the presence of further reactants or products. Thus, dynamic effects are a priori absent, and the physical picture where promoting species are strongly depleted may be different. However, the existence of a solid framework that is able to explain numerous experimental results [7] indicates that the role of promoters can be understood beyond the particular chemicals present on the surface. On the other hand, in the case of the Monte Carlo simulations, the spillover effect is implicit in the changes in chemical potential. A more positive chemical potential emulates the pumping of promoters to the catalyst surface. In the case of quantum mechanical calculations, the increase in chemical potential is not straightforwardly introduced, but emulated by an increasing coverage degree of the ad-species. In this case, a higher coverage degree represents a larger chemical potential.

2 Model and computations

2.1 DFT calculations

Density Functional Theory (DFT) calculations were performed employing the SIESTA computer code [9, 10]. A localized basis set composed of double$-\zeta$ plus polarization was used. The basis functions were numerical atomic orbitals (NAOs), the solutions of the Kohn-Sham's Hamiltonian for the isolated pseudoatoms. Exchange and correlation effects were described using a generalized gradient approximation (GGA), within the Perdew–Burke–Ernzerhof (PBE) functional [11]. The core electrons were replaced by norm conserving pseudopotentials [12] in their fully separable form [13]. The non-linear exchange-correlation correction [14] was included for Pt to improve the description of the core valence interactions. In the pseudopotential description of the atoms, the following valence electronic states were considered: Pt:$6s^1 5d^9 6p^0$; O:$2s^2 2p^4$; Na:$3s^1 3p^0$. In order to obtain orbitals with continuous derivatives, a soft confinement potential was employed [15]. The value of the confinement parameters were defined variationally applying the simplex method [16]. All the parameters used in the calculations are listed in Table 1.

As the SIESTA code employs NAOs, the program replaces some integrals in real space by sums in a finite three dimensional (3D) real space grid, controlled by one single parameter, the energy cutoff of the grid [9]. This cutoff, which refers to the fineness of the grid, yielded converged results for all the systems studied here at 150 Ry. All the calculations were performed with spin polarization (sp).

The catalyst surface was represented by a bare Pt(111) slab made of two Pt layers of 16 atoms. The unit cell was a 10.93 Å $\times$ 10.93 Å $\times$ 20 Å hexagonal one, and periodic boundary conditions in x, y, z directions were imposed in order to represent an infinite surface.

In the case of the oxidized substrate surface, an ordered submonolayer of oxygen adsorbed on Pt(111) was represented by four O atoms adsorbed on fcc-hollow sites of the Pt(111) surface, yielding a $p(2 \times 2)$ superlattice (coverage degree = 0.25).

The charges on the different atoms were evaluated by means of the Mulliken population analysis [8].

Table 1 r_{nl} Represents the cutoff radius of the potentials

In the basis, the single and double zeta orbitals of a given angular momentum have the following parameters: r_1, $r_{c,1}$, $r_{c,2}$ which are the inner radius, the cutoff radius of the first and second zeta for a given angular momentum, respectively. All radiuses are expressed in [Bohrs]. δQ, V_0 represent the extra charge [a.u.] and the prefactor of the soft confinement potential [Ry], respectively

Symbol	Potential	Basis	
		δQ	Soft confinement parameters
O	r_{2s} 0.89 r_{2p} 0.89 r_{3d} 1.00 r_{4f} 1.29	0.019	$2s$: V_0 0.86, r_i 3.00, $r_{c,1}$ 6.53, $r_{c,2}$ 2.87 $2p$: V_0 0.08, r_i 6.70, $r_{c,1}$ 7.74, $r_{c,2}$ 2.77
Na	r_{3s} 2.95 r_{3p} 3.50 r_{3d} 2.95 r_{4f} 2.95	0.150	$3s$: V_0 149.92, r_i 6.46, $r_{c,1}$ 8.02, $r_{c,2}$ 6.43 $3p$: V_0 150.00, r_i 6.03, $r_{c,1}$ 7.98
Pt	r_{6s} 2.35 r_{6p} 2.40 r_{5d} 1.24 r_{5f} 2.35	0.065	$6s$: V_0 35.24, r_i 6.53, $r_{c,1}$ 7.74, $r_{c,2}$ 5.52 $6p$: V_0 10.23, r_i 2.02, $r_{c,1}$ 7.53 $5d$: V_0 30.99, r_i 6.64, $r_{c,1}$ 7.48, $r_{c,2}$ 5.53

To study the minimum energy configuration of the system in the presence of different adsorbates, local minima were analyzed through the conjugate gradient technique [16]. This was performed initially locating the adsorbate at some point on the unperturbed surface of the metal, and then minimizing the energy of the system with respect to all the atomic coordinates. While this method is suited to study local minima, it does not yield information on global minima. Thus, structures with major rearrangements of the surface were not studied, and will be analyzed in the future by computational techniques involving a finite temperature of the system.

2.2 Monte Carlo simulations

Monte Carlo simulations on the adsorption of ions on a charged surface were also performed, so as to emulate the formation of the above mentioned electrostatic double layer. Figure 1 shows the model employed here, where the metal was considered as a perfect conductor and the Na^+ ions were allowed to interact with the surface through their image charge. A hard core represented the repulsion of the core electrons with the corresponding metal core ions.

The z axis is perpendicular to the charged wall. Four different approximations were used to deal with the long-range interactions arising in the model: normal Coulomb; Shifted Potential (SP); Shifted Force (SF) and Damped Shifted Potential (DSP).

These interatomic potentials [17] have the following functional form:

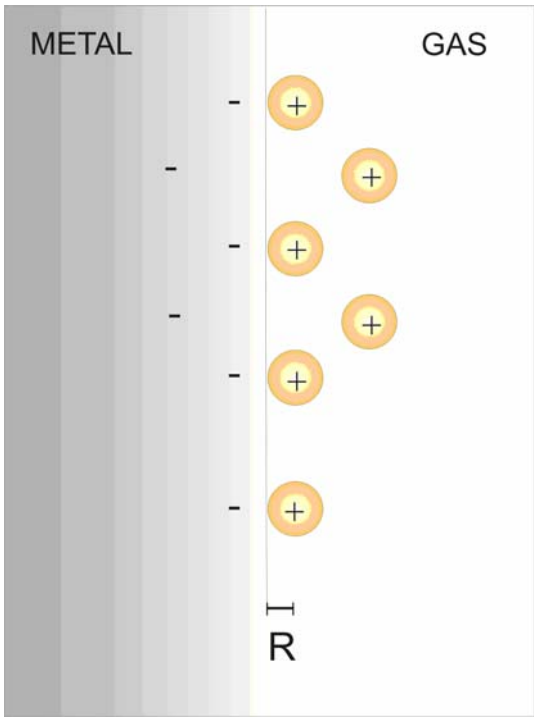

Fig. 1 Scheme representation of the metal–catalyst/gas interface

The normal Coulomb (C) potential;

$$V(r) = \frac{q_i q_j}{r_{ij}}$$

the Shifted Coulombic Potential (SP);

$$V_{\mathrm{SP}}(r) = q_i q_j \left(\frac{1}{r} - \frac{1}{R_c}\right), \quad r \le R_c$$

where R_c is the radius at which the potential is turned off; the Shifted Force (SF) Coulomb potential;

$$V_{\mathrm{SF}}(r) = q_i q_j \left[\frac{1}{r} - \frac{1}{R_c} + \left(\frac{1}{R_c^2}\right)(r - R_c)\right], \quad r \le R_c$$

and Damped Shifted Potential (DSP) ones

$$V_{\mathrm{DSP}} = q_i q_j \left[\frac{erfc(\alpha r)}{r} - \frac{erfc(\alpha R_c)}{R_c} + \left(\frac{erfc(\alpha R_c)}{R_c^2} + \frac{2\alpha}{\pi^{1/2}} \frac{\exp\left(-\alpha^2 R_c^2\right)}{R_c}\right)(r - R_c)\right], \quad r \le R_c$$

where a damping function is incorporated in order to muffle the potential and to accelerate the convergence. In this equation, α is the damping or convergence parameter with units of $\mathrm{Å}^{-1}$.

A rectangular simulation box was employed with sides L_x, L_y and L_x. In the present simulations, we used $L_y = 5$ nm, $L_z = 1.5$ nm, and L_x was chosen so that $L_x = 2L_y\cos(30°)$. Periodic boundary conditions in the x–y directions were applied.

The computer simulations were carried out by means of an off-lattice simulation scheme in the Grand Canonical ensemble [18], where the chemical potential of Na^+ ions, the volume of the system and the temperature are fixed in order to emulate the experimental conditions. The potential energy and the number of Na^+ ions fluctuated according to the different type of events allowed:

1. Particle displacement Na^+, using as acceptance ratio:
   $$W_{i\to j} = \min\left(1, \exp\left(-v_{ij}/kT\right)\right)$$
   where v_{ij} is the change of potential energy related to the configuration change $i \to j$.
2. Insertion of the Na^+ ion: a particle is randomly inserted into the simulation box and the new configuration is accepted according to:
   $$W_{N\to N+1} = \min\left(1, \frac{V}{\Lambda^3(N+1)} \exp\left(\left(\mu - \Delta v_{N+1,N}\right)/kT\right)\right)$$
   where V is the volume to which the particles have access, $\Lambda = \sqrt{\frac{h^2}{2\pi mkT}}$ is De Broglie thermal wavelength,

and $\Delta v_{N+1,N} = v_{N+1} - v_N$ denotes the potential energy difference which results from the attempt to create a particle.

3. Removal of a Na^+ ion: a Na^+ atom randomly selected is removed from the system and the new configuration is accepted according to:

$$W_{N\to N-1} = \min\left(1, \frac{\Lambda^3 N}{V}\exp\left(\left(-\mu - \Delta v_{N-1,N}\right)/kT\right)\right)$$

with $\Delta v_{N-1,N} = v_{N-1} - v_N$.

3 Results and discussion

3.1 DFT study of the Na adsorption

Figure 2 shows the Na-$p(2\times2)$/Pt(111) equilibrium structure minimized by the conjugate gradient (CG) technique. The Na adatom is adsorbed on an fcc-hollow site. The average distance $\overline{d_{Pt-Na}}$ to the nearest neighbors is 2.96 Å, with a binding energy of −2.30 eV and a positive charge of 0.41 [a.u.]. These important charges on the adsorbates induce negative image charges on the surface that gives place to a double layer of charge, so that the energy levels are displaced towards more positive values. This should also be reflected in the density of states (DOS) of the system. The density of states per unit energy E (and per unit volume Ω_{cell} in extended matter) is the number of states [19] defined according to the equation:

$$\mathrm{DOS}(E) = \frac{\Omega_{cell}}{(2\pi)^d}\int_{BZ} dk\,\delta\left(\varepsilon_{i,k} - E\right)$$

where $\varepsilon_{i,k}$ denotes the energy of an electron in an independent-particle state and d is the space dimension.

The changes in the density of states can be appreciated in Fig. 2, as well as the shift of the Fermi level from −4.30 eV (Pt) to −2.68 eV (Na/Pt). This surface charge transfer produced by the Na adsorbates, located at a distance of 2.44 Å from the first Pt plane, gives an increase of the Pt–Pt inter-planar distance from 2.46 to 2.49 Å.

At the lower coverage of 0.0625, the Na atoms at the Na-$p(4\times4)$/Pt(111) structure present a larger ionic binding, equal to −2.77 eV and the charge rises to 0.62 [a.u.]. It becomes more distant from the three nearest Pt neighbors ($\overline{d_{Pt-Na}} = 3.05$ Å) than in the case of the $p(2\times2)$ structure. The Fermi level is shifted to −3.70 eV, a lower value than of the $p(2\times2)$ case. This can be related to the fact that at a lower coverage, the induced surface charge dipole at the interface decreases.

Table 2 summarizes the results for the charge on a Na atom and its binding energy on Pt(111) according to DFT calculations at different coverage degrees, in comparison with results from the literature. It can be observed that the partial charge on the atom increases for decreasing coverage degrees. On the other hand, the binding becomes stronger, in all cases being the binding energy lower than the cohesive energy of bulk Na $E_{cohesive}^{Na,metal} = -1.08$ eV (DFT) [20], −1.11 eV (experimental) [21]. In order to

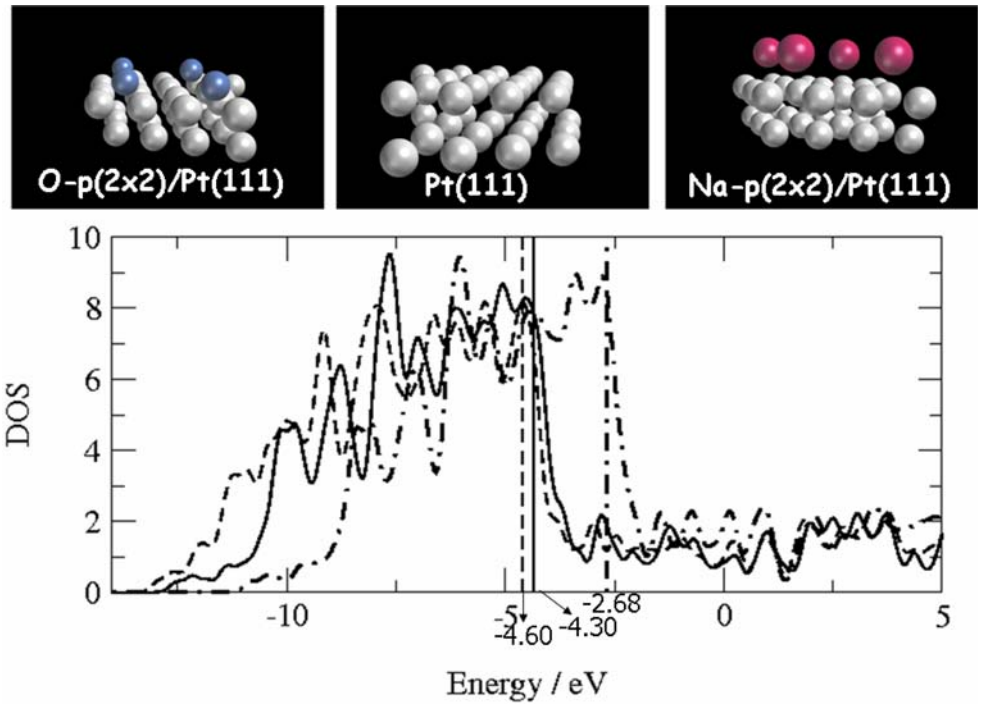

Fig. 2 (Top) DFT equilibrium structures for the O-$p(2\times2)$/Pt(111), Pt(111) and Na-$p(2\times2)$/Pt(111). (Magenta) Na; (blue) O; (grey) Pt atoms, respectively. (Bottom) Densities of States (DOS) as function of the energy. (Dashed line) O-$p(2\times2)$/Pt(111), (full line) Pt(111), (dot-dashed line) Na-$p(2\times2)$/Pt(111)

Table 2 Charge and binding energy of a Na atom on Pt(111) at different coverage degrees according to the present results and the literature [20]

Θ	μ (Debye)	$Q_{Na^+} = \mu$ (d_{Pt-Na})	Q_{Na^+}(Mulliken) (a.u.)	E_{bind} (eV)
0.33 (1)	1.8 [20]	0.16 [20]		−2.36
0.25 (2)	2.3 [20]	0.205 [20]	0.41	−2.48 [20]/ −2.30
0.0625 (3)			0.62	−2.77

In the case of the results reported from reference [20], the charges were estimated from the dipole moment μ and the Pt–Na distance d_{Pt-Na}. For the different coverages, the structures are (1) Na−$\left(\sqrt{3}\times\sqrt{3}R30^\circ\right)$/Pt(111); (2) Na-$p(2\times2)$/Pt(111); (3) Na-$p(4\times4)$/Pt(111)

Table 3 Charge on a Na atom (Mulliken) and binding energy on a O-(2×2)/Pt(111) surface according to DFT calculations

Θ	Q_{Na^+}(Mulliken) (a.u.)	E_{bind} (eV)
0.0625 (1)	0.79	−3.03

(1) Corresponds to a Na-$p(4\times4)$–O-$p(2\times2)$/Pt(111) structure

come closer to the experimental conditions, the adsorption of Na atoms was also considered on a O-$p(2\times2)$/Pt(111) surface with the results presented in Table 3. It can be seen that the binding on an oxide-covered surface is stronger and that the charge transfer becomes even larger.

3.2 MC simulations of the Na adsorption

The large charges on the Na atom found in the previous section support the assumption of an *ionic binding* of the Na atom to a O-$p(2\times2)$/Pt(111) surface. Ionic interactions involve the existence of long-ranged coulombic potentials that may lead to complications if improperly truncated. In order to prove this point, we have performed extensive simulations at different chemical potentials with the four different versions of coulombic interactions described above: Coulomb (truncated at the borders of the simulation box); Shifted Potential (SP); Shifted Force (SF) and Damped Shifted Potential (DSP). Figure 3 shows the coverage degree as a function of the chemical potential from simulations carried out with these interaction potentials. Most importantly, the qualitative predictions are similar in all cases, independently of the truncation scheme applied.

Snapshots of the configurations obtained from the MC simulations for the Na/catalyst surface at three different chemical potentials are shown in Fig. 4a, where it is found that as the coverage degree increases, the systems become progressively ordered.

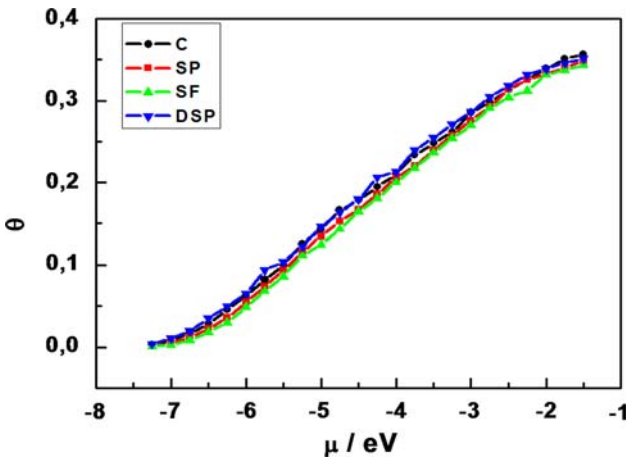

Fig. 3 Coverage degree (Θ) of adsorbed species as a function of the chemical potential (μ) for the different potentials employed

From the simulation it becomes evident that the adsorbates ions are more or less confined close to a plane parallel to the surface defined by the substrate. Thus, it seems appropriate to define the following pair distribution function as:

$$g(r_{||}) = \frac{S}{N^2}\left\langle \sum_i \sum_{j\neq i} \delta\left(r_{||} - \left\|\overrightarrow{r_{ij}}\right\|\right)\right\rangle$$

where $\left\|\overrightarrow{r_{ij}}\right\|$ is the projection onto the plane parallel to the surface of the vector $\overrightarrow{r_j} - \overrightarrow{r_i}$ joining the particles, and S denotes the surface of the system [22]. The averages are taken over cylindrical shells and the distribution function is referred to as an ideal gas with the average surface density N/S. In the present case, the average was calculated from histograms for distances in the range $0 < r_{||} \leq 2.5$ nm.

Figure 4b shows that $g(r_{||})$ presents a series of peaks that become more resolved as the chemical potential increases. These peaks correspond to the first, second, third, etc. nearest neighbors of an ordered distribution.

Furthermore, to complete our structural characterization, we also calculated $g(\alpha)$, the angular distribution function of neighbors around a site within a plane up to a certain distance. The function $g(\alpha)$ allows the possibility of having two neighbors of an atom forming an angle (α). The $g(\alpha)$ obtained in the present simulation, shown in Fig. 4c, suggests the occurrence of a hexagonal lattice of ions at large chemical potentials.

The results of the present section can be summarized stating that a crossover between a disordered and an ordered state can be detected from the Monte Carlo Grand Canonical simulations with different versions of an ionic model for adsorption. While the isotherm shows no evidence for the existence of a first-order phase transition, a more detailed study using different system sizes and

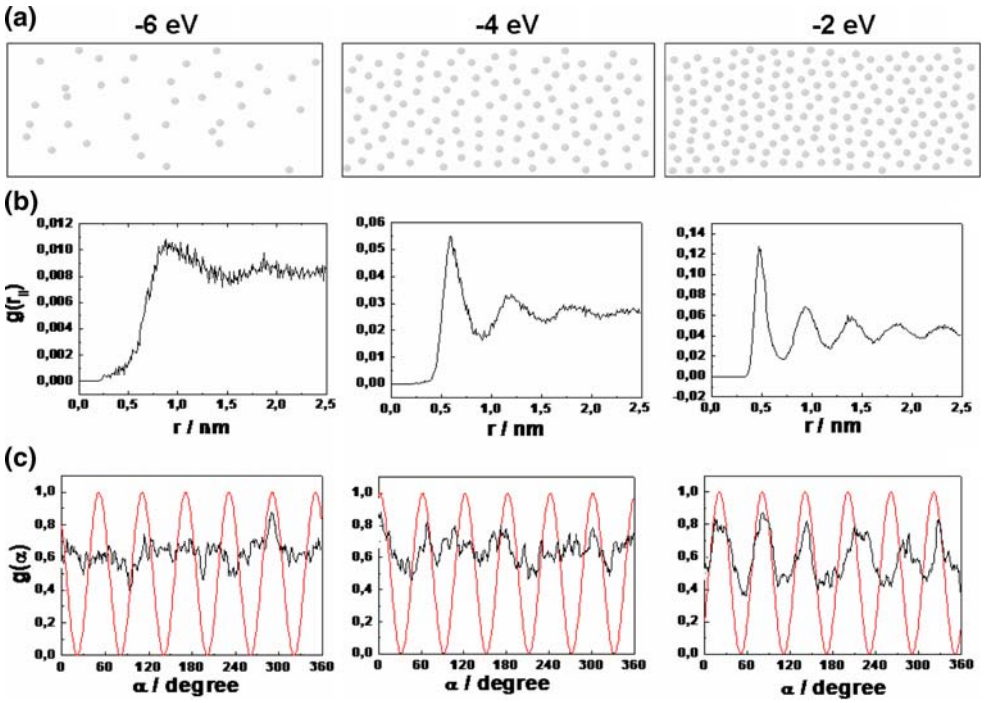

Fig. 4 Results of MC simulations for an ionic model for the catalyst–gas interface. Three different applied chemical potentials are shown. (Upper) Configurations where each dot represents an adatom. (Middle) Radial distribution functions. (Lower) Angular distribution functions. The continuous (large-amplitude) lines, are drawn to emphasize the angular dependence

temperatures is required in order to analyze the possibility of a second-order phase transition.

3.3 DFT study of the O adsorption

The adsorption of O and O_2 species was also considered by DFT calculations. The magnitude of the partial charges on O is lower than those reported above for Na. Q_0 is typically of the order of -0.43 in the case of (O(2×2)) and of the order of -0.45 for the (O(2×2) + additional O) structure, but the introduction of further O atoms leads to an noticeable strain of the Pt surface.

The adsorption of O atoms on the Pt(111) surface yielding a O-$p(2 \times 2)$/Pt(111) supercell, as shown in Fig. 2, results in a binding energy -3.39 eV per O atom, with a charge of -0.43 a.u. The negative charges of the adsorbates induce positive image charges on the surface that gives place to a double layer of charge, so that the energy levels are displaced towards more negative values. This fact can be appreciated in the density of states plot of Fig. 2, and in the displacement of the Fermi level from -4.30 eV (Pt) to -4.60 eV (O/Pt). This surface charge transfer produced by the O adsorbates, located at a distance of 1.31 Å from the first Pt plane, causes a decrease in the Pt–Pt inter-planar distance from 2.46 to 2.44 Å.

In order to emulate further the O adsorption on the surface, a $p(4 \times 4)$/Pt(111) unit cell was considered, with O atoms forming four units O-$p(2 \times 2)$/Pt(111) superstructure as in the previous case. On this supercell, an additional O atom was adsorbed on an fcc-hollow adsorption site, as depicted in Fig. 5a. We will denote this additional adsorbed O species with O*. The resulting

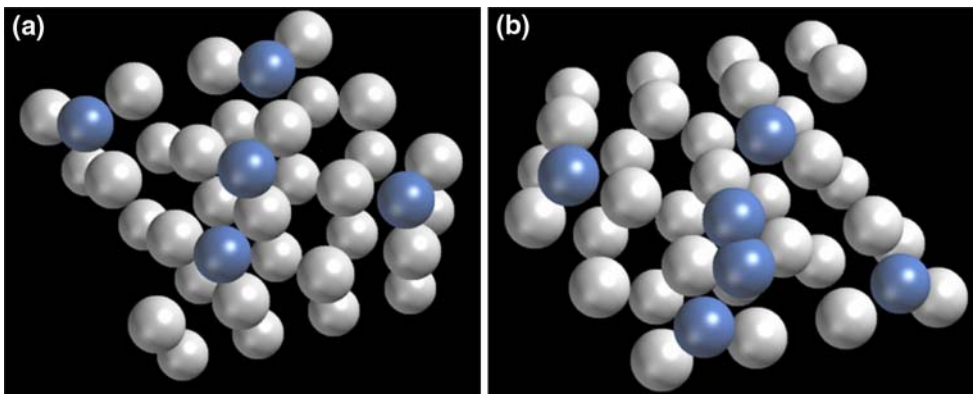

Fig. 5 (**a**) O; (**b**) O_2 adsorption on free fcc-hollow site of the O-$p(2 \times 2)$/Pt(111) surface

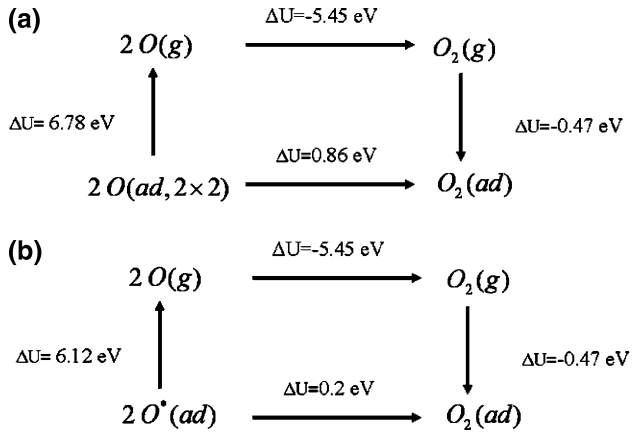

Fig. 6 Born-Haber cycle used to analyze the possibility of coexistence of different species on the O-$p(2 \times 2)$–Pt(111) surfaces (**a**) Corresponds to O species forming part of the O-$p(2 \times 2)$/Pt(111) structure; (**b**) Corresponds to O species further adsorbed on a pre-existing O-$p(2 \times 2)$/Pt(111) structure

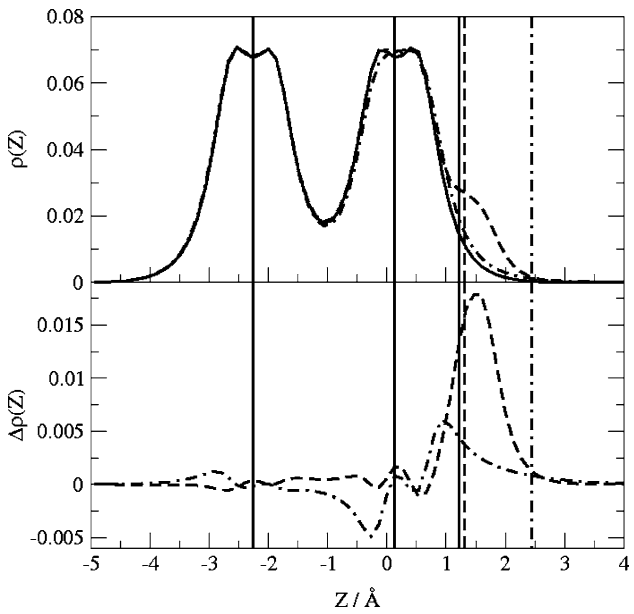

Fig. 7 (Top) Electronic density vs. z-direction. (Bottom) Difference of electronic densities with respects to the Pt one. (full line) Pt; (dashed line) O-$p(2 \times 2)$/Pt(111); (dot-dashed line) Na-$p(2 \times 2)$/Pt(111)

binding energy was -3.06 eV, and the corresponding charge was -0.45 a.u.

O_2 adsorption on the O-$p(2 \times 2)$/Pt(111) supercell yielded a binding energy of -0.47 eV, having each atom of the oxygen molecule a charge of -0.15 a.u.

With the previous data, a Born-Haber cycle can be constructed as shown in Fig. 6a to analyze which species may be present on the surface. The cycle in part (a) shows that O_2 may adsorb on the oxide surface but that is unstable with respect to the formation of the O-$p(2 \times 2)$/Pt(111) structure. In other words, considering a surface that is partially covered with a O-$p(2 \times 2)$/Pt(111) structure O_2 may adsorb on it and dissociate contributing to the further growth of the oxide layer. On the other hand, the cycle in Fig. 6b indicates that some equilibrium may exist between the additional O* species and the O_2 molecule.

The fact that in all cases the atomic oxygen species are more stable than the molecule is consistent with the experimental fact that oxygen adsorption on Pt is dissociative under EPOC conditions (Electrochemical Promotion of catalysis), i.e. at high temperatures, where kinetic hindrances are diminished.

Figure 7 (upper) illustrates the electronic density averaged over the x–y plane, named $\rho(z)$ as a function of the z-direction for different systems, while Fig. 7 (lower) shows differential plots $\Delta\rho(z)$, where this quantity is defined according to:

$$\Delta\rho(z) = \rho_{\mathrm{A/Pt(111)}} - \rho_{\mathrm{Pt(111)}}$$

where $\rho_{\mathrm{A/Pt(111)}}$ and $\rho_{\mathrm{Pt(111)}}$ are the electronic densities of the adsorbate/Pt(111) and pure Pt(111) systems respectively. Specifically, since the present calculations employ pseudopotentials, we should rather use the term pseudo-electronic densities. For the sake of simplicity, we leave out in the following the term pseudo, but this difference should be noted, since in the core region, the pseudoelectronic density does not have a straightforward physical relevance. Vertical lines are also drawn in Fig. 7, denoting some important locations in the system. The full vertical lines at the centre of the figure denote the position of the Pt lattice planes. The full line on the right indicates the ideal position of the metal edge, which is located at half the distance between lattice planes from the first plane of Pt atoms (Jellium edge). This position corresponds to the plane where an external charge should be mirrored in order to draw the classical electrostatic image charge picture of the problem. If the metal was a perfect conductor, any external charge should be screened by inducing a Dirac-delta charge distribution at this point. The dashed and the dot-dashed vertical lines indicate the position of the O and the Na adsorbate planes, respectively. The full lines in the upper part of Fig. 7 indicate the density $\rho(z)$ for the clean Pt(111) slab. Both maxima correspond to the location of the Pt lattice planes. When the O-$p(2 \times 2)$ and Na-p (2×2) adsorbates are added to the system, the electronic density of the system changes as shown in the lower part of Fig. 7. A striking difference between the O and the Na adsorbates is evident. While in the case of O a maximum in the differential electronic density occurs close to the position where the adsorbates are located (see vertical dashed line), in the case of the Na adsorbate the maximum is close to the location of the ideal image plane (vertical full line on the right). On the other hand, at the position of

the Na adsorbate there is practically no indication of a remaining electronic density. This shows that the Na atom has been strongly depleted from its electronic density, being the latter displaced to the metal surface. In order to screen the field produced by the presence of the Na ions, the metal induces a negative charge on its surface. Other oscillations are present in the system, as is typical for the screening of a perturbation in an electronic gas. A small maximum in the electronic density occurs at the back side of the system (clean Pt(111) surface). This results from the presence of two surfaces with different work functions in this system. Since the work function of the Na-$p(2 \times 2)$ surface is lower, it accumulates positive charge, while the opposite occurs with the other surface.

Figure 8 shows, for the different systems, the x–y averaged electrostatic potential $V(z)$, the difference $\Delta V(z)$ with respect to the clean Pt(111) surface and the electric field $E(z)$ as a function of the z-direction. If the centre of the slab is used as a reference, it is found that the introduction of the Na-$p(2 \times 2)$ overlayer produces an increase in the electrostatic potential of ca. 0.35 eV, while the O-$p(2 \times 2)$ overlayer induces a decrease of −0.07 eV. These figures provide a rough estimation for the work function changes of the Pt(111) surface in the presence of the different adsorbates.

The O-$p(2 \times 2)$ structure produces a maximum in the field of 0.83 [V/Å] at the interface. On the other hand, the Na-$p(2 \times 2)$ structure yields a minimum (field pointing towards the surface of −0.16 [V/Å]).

A linear change in the potential is evident outside the metal slab since both surfaces of the system present different work functions, as stated above. The corresponding field can be used to make a further estimation of the work function difference between the clean and the adsorbate-covered Pt(111) surface. It is well known that when two metal surfaces with different work functions are brought in contact, a potential difference between the two surfaces develops. Thus, we can estimate the work function difference $\Delta\Phi_{A/Pt(111)}$ between the two surfaces from:

$$\Delta\Phi_{A/Pt(111)} = eE\Delta x$$

where E is the field well outside the metal slab, and Δx is the effective distance between the two metal surfaces. Estimating Δx as the box length in the z direction minus two times the distance between Pt(111) lattice planes, we obtain $\Delta\Phi_{Na\text{-}p(2\times2)/Pt(111)} = 0.40\,eV$ and $\Delta\Phi_{O\text{-}p(2\times2)/Pt(111)} = -0.06\,eV$, in a reasonable agreement with the previous estimations. A more precise estimation of the work function can be made, as discussed in reference [23], but a considerably larger system (thicker slab) should be employed for a quantitative calculation.

Figure 9 shows that this field increases up to 1.01 V/Å when additional O* atoms are adsorbed on the oxide surface, giving place to the beginning of some Pt

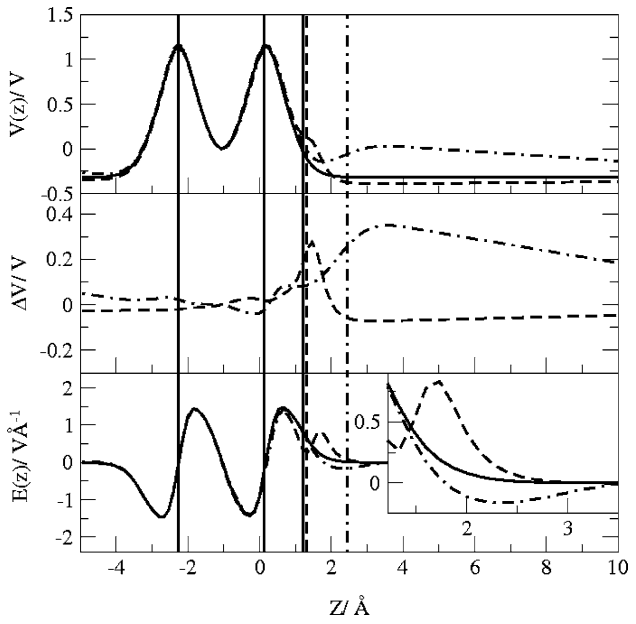

Fig. 8 (Top) Average electrostatic potential [V] vs. z-direction; (Middle) electrostatic potential difference [V] referred to the one of the pure Pt(111) slab. (Bottom) Electric Field [V/Å]. (Inset) Magnification of the field at the interface. (full line) Pure Pt(111) slab; (dashed line) O-$p(2 \times 2)$/Pt(111); (dot-dashed line) Na-$p(2 \times 2)$/Pt(111)

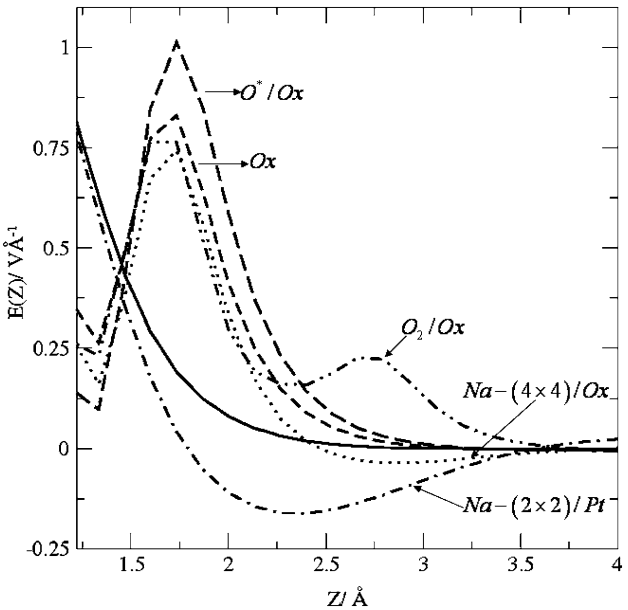

Fig. 9 Electric Field [V/Å] at different catalyst/vacuum interfaces. (full line) Pure Pt(111) slab ; (short-dashed line) O-$p(2 \times 2)$/Pt(111); (dot-dashed line) Na-$p(2 \times 2)$/Pt(111); (long-dashed line) O*—O-$p(2 \times 2)$/Pt(111); (dot-dot-dashed line) O_2—O-$p(2 \times 2)$/Pt(111); (dotted line) Na-$p(4 \times 4)$–O-$p(2 \times 2)$/Pt(111). In the figure, the shorthand notation "Ox" is used to denote the O-$p(2 \times 2)$/Pt(111) structure

rearrangement at the surface. In the case of the O_2 adsorption, a new maximum appeared on the field profile which produces even more important rearrangements than in the O adsorption case.

4 Conclusions

- DFT calculations show that Na atoms have high positive charges when adsorbed on high work function substrates (like Pt(111)). The ionic nature of the binding induces a negative image charge on the surface and produces an important decrease in the work function.
- The Na adatoms acquire even more positive charges when they are adsorbed on surfaces with a higher work function (like O/Pt(111)).

These results suggest that the ionic binding model may be applied to the present system.

- Na/substrate Monte Carlo simulations, in term of an ionic model, show a crossover from a *disordered* to an *ordered* state of ad-species as the coverage degree is increased. The same qualitative features are observed, independent from the truncation scheme applied to the electrostatic interaction potentials.
- We have considered by means of DFT calculations two type of atomic oxygen species adsorbed on platinum surfaces. According to Mulliken population analysis, they have a charge of the order of -0.43 when adsorbed on the Pt(111) surface. The ionic nature of the binding induces a positive image charge on the surface which produces an important increase of the work function. Molecular O_2 adsorbed on the oxidized platinum surface presents a charge of -0.15 a.u./atom.
- Na and O adsorbates show opposite trends concerning the relaxation of the Pt lattice upon adsorption. While Na seems to generate an expansion of the Pt lattice caused by the electron transfer to the metal, O induces a compression due to the opposite effect. This may be relevant for determining the accessible metallic fraction of Pt in the catalysts, a crucial parameter in catalysis. However, real catalysts present structures that are rough in the microscopic scale, so that calculations with stepped or imperfect surfaces are required in order assess this effect accurately.
- The adsorption of O; O_2 induce surface rearrangement of the Pt(111) surface. This situation may be the onset of the formation of other more stable adsorbed oxygen species. Future work should consider the possibility of the formation of other oxygen species that may be globally more stable than those studied here, as well oxygen adsorption on stepped surfaces. This situation would represent a more realistic approximation to the experimental catalyst than the perfect Pt surfaces considered here.

Acknowledgments This work was supported by PIP 5901/05 CONICET, Program BID 1728/OC-AR PICT 06-12485, Agencia Córdoba Ciencia and SECyT UNC, Argentina. We wish to thank C. Mosconi for language assistance.

References

1. Vayenas CG, Bebelis S,Yentekakis IV, Lintz HG (1992) Catal Today 11:303
2. Makri M, Bebelis S, Vayenas CG, Besocke K, Cavalca C (1996) Surf Sci 369:351
3. Vayenas CG, Archonta D, Tsiplakides D (2003) J Electroanal Chem 554–555:301
4. Vayenas C, Brosda S (2002) Solid State Ionics 154–155:243
5. Vayenas CG, Brosda S, Pliangos C (2003) J Catal 216:487
6. Vayenas CG (2004) Solid State Ionics 198:321
7. Brosda S, Vayenas CG (2002) J Catal 208:38
8. Szabo A, Ostlund NS (1989) Modern quantum chemistry. Graw-Hill, New York, pp 151
9. Ordejón P, Artacho E, Soler JM (1996) Phys Rev B 53:R10441
10. Soler JM, Artacho E, Gale JD, García A, Junquera J, Ordejón P, Sánchez-Portal D (2002) J Phys: Condens Matter 14:2745
11. Perdew JP, Burke K, Ernzerhof M (1996) Phys Rev Lett 77:3865
12. Troullier N, Martins JL (1991) Phys Rev B 43:1993
13. Kleinman L, Bylander DM (1982) Phys Rev Lett 48:1425
14. Louie SG, Froyen S, Cohen ML (1982) Phys Rev B 26:1738
15. Junquera J, Paz O, Sánchez-Portal D, Artacho E (2001) Phys Rev B 64:235111
16. Press WH, Flannery BP, Teukolsky SA, Vetterling WT (1986) Numerical recipes: the art of scientific computing. Cambridge University Press, Cambridge, England
17. Fennell CJ, Gezelter JD (2006) J Phys Chem 124:34104
18. Frenkel D, Smit B (1996) Understanding molecular simulations. Academic Press, London, 101 pp
19. Martin RM (2004) Electronic structure. Cambridge University Press, Cambridge, UK, 96 pp
20. Moré S, Seitsonen AP, Berndt W, Bradshaw AM (2001) Phys Rev B 63:75406
21. Kittel C (1986) Introduction to solid state physics. Wiley, New York, USA
22. Allen MP, Tildesley DJ (1992) Computer simulation of liquids. Oxford University Press, New York, USA, 55 pp
23. Junquera J, Cohen MH, Rabe KM (2007) J Phys: Condens Matter 19:213203